ELSEVIER

Contents lists available at ScienceDirect

# Computers and Fluids

journal homepage: www.elsevier.com/locate/compfluid





# Effect of Local Thermal Strips on Hypersonic Boundary-Layer Instability

Jaeyoung Park <sup>a</sup>, Prasanna Thoguluva Rajendran <sup>b</sup>, Minwoo Kim <sup>c</sup>, Jiseop Lim <sup>c</sup>, Solkeun Jee <sup>c</sup>, Donghun Park <sup>a</sup>, <sup>\*</sup>

- <sup>a</sup> Department of Aerospace Engineering, Pusan National University, Busan, South Korea
- <sup>b</sup> Department of Aerospace and Mechanical Engineering, The University of Arizona, Tucson, Arizona, U.S.A
- <sup>c</sup> School of Mechanical Engineering, Gwangju Institute of Science and Technology, Gwangju, South Korea

#### ARTICLE INFO

# Keywords: Hypersonic Boundary layer Linear stability theory (LST) Instability Transition Thermal strip

#### ABSTRACT

An effect of localized thermal strips on hypersonic boundary-layer instability is investigated using linear stability theory (LST). The linear evolution of Mack's second mode is analyzed for a Mach 4.5 flat-plate boundary-layer with and without the strips. The validity of the LST analysis is assessed through the comparison of the results with implicit large eddy simulations (ILES) for selected cases. Parametric studies on the temperature intensity, length, and location of a single strip are performed to examine the influence of the strip on the second-mode instability. A reversal in the stabilizing and destabilizing effect according to the local streamwise surface pressure gradient induced by the strip is identified. The reversal point of the stabilizing/destabilizing effect is located in the vicinity of the location of the maximum growth rate of the second mode. The influence of three strips in a series arrangement is also analyzed for several combinations. The proper combination of strips, considering the reversal phenomenon, results in more significant stabilizing/destabilizing effects for a disturbance with a specific frequency. The overall effects are also evaluated and analyzed in terms of the envelope of the N-factor curves by carrying out the LST calculations for disturbances with various frequencies.

# 1. Introduction

The boundary-layer transition possesses a first-order impact on aerothermodynamic performance and flight stability; therefore, understanding and predicting a transition is essential for the design and analysis of hypersonic vehicles because a significant portion of their flight time is subject to the transitional boundary-layer regime [1]. The presence of a fully turbulent boundary-layer is typically assumed when designing a high-speed flight vehicle. However, aerodynamic heating on the vehicle's surface is higher by eight times or more in the turbulent boundary-layer. Specifically, it could cause a severe thermal problem in the transitional regions at hypersonic Mach numbers [2]. The vehicle's surface may be composed of various elements with materials of different thermal conductivities. Diversity in surface materials may cause a temperature variation along the streamwise direction during the flight, and this eventually affects the hypersonic boundary-layer instability and transition. Thus, it is necessary to predict a transition onset concerning streamwise variations of surface temperature for the optimal aero-thermodynamic design of a hypersonic vehicle.

Several studies have analyzed the instability of the hypersonic

boundary-layer with wall-temperature variations. The effect of heat transfer on the instability of the two-dimensional hypersonic boundarylayer was first studied by Mack [3]. The study showed that first-mode instabilities are destabilized by heating over the entire surface, whereas Mack's second-mode instabilities, known as a dominant mechanism leading to the hypersonic boundary-layer transition, are destabilized by cooling. Subsequently, Masad and Abid [4] demonstrated the transition reversal phenomenon using the opposite effects of surface heating/cooling on the first/second-mode instabilities. Soudakov et al. [5] focused on local surface temperature variations and performed a direct numerical simulation (DNS) of a hypersonic boundary-layer on a flat plate at Mach 6. They observed compression and expansion waves near the regions of positive and negative jumps in temperature, respectively. It was confirmed that these features essentially change the stability and receptivity process. The research on a single local heating/cooling strip on the hypersonic boundary-layer instability first began with experiments and numerical simulations performed by Soudakov. By carrying out the experiment and numerical simulation for a 7-degree half-angle cone at Mach 6, Sidorenko et al. [6] identified that the development of the second mode depends on the

E-mail address: parkdh@pusan.ac.kr (D. Park).

<sup>\*</sup> Corresponding author:

upstream wall temperature, and observed that variation of the wall temperature significantly affects the transition location. Fedorov et al. [7] studied the localized surface heating or cooling effects on the stability of the boundary layer for the same geometry but under different conditions. They examined two-dimensional disturbances propagating in a boundary layer passing over a region of cooling/heating of different intensities by conducting a wind-tunnel experiment and DNS, and observed that the localized cooling attenuates the second-mode amplitude and thus delays transition. Zhao et al. [8] also numerically investigated the effect of a single local heating/cooling strip on a flat plate at Mach 6 and confirmed that the relative location of the strip to the synchronization point, where the mode F and mode S are synchronized, significantly affected the second mode instability. It was the first study to observe that the unstable mode is amplified when a heating strip is located upstream of the synchronization point, and the effect is reversed if the heating strip is placed downstream of it. Batista and Kuehl [9] performed a numerical study on a flared cone at Mach 6 for which the wall temperature varies along the downstream direction. Their results showed that wall heating immediately downstream of the first neutral point amplifies the second mode, whereas the heating further downstream dampens it. Zhao and Dong [10] recently studied the effect of local surface thermal strips on Mack's second mode in a supersonic and hypersonic boundary-layer. In his work, a systematic study for different control parameters is carried out based on an asymptotic analysis, and it is confirmed that a heating strip enhances/suppresses the second mode with frequencies below/above a critical value, while a cooling strip shows the opposite influences. They also observed that the critical frequency, which causes the reversed impacts of the thermal strip, is the most unstable frequency of Mack's second mode, instead of the synchronization frequency found in some previous works for both roughness and temperature-strip.

There have been many studies on the effects of heating/cooling strips on hypersonic boundary-layer instability. From several previous research [8-10], reversed effect depending on the location of the strip has been reported, and it is observed that the critical frequency corresponds to the most unstable frequency. However, a more detailed parametric study on a localized thermal strip is necessary to seek a comprehensive explanation of the reverse effect on the second mode instability. Furthermore, to the author's knowledge, the combined impact of sequentially arranged multiple strips is rarely studied. In this study, the effect of a single local heating/cooling strip and its multiple combinations on Mack's second-mode instability in a hypersonic boundary-layer is assessed by using spatial linear stability theory (LST). A parametric study on a single strip is carried out, and its influence on Mack's second-mode instability obtained from LST analysis is validated using an implicit large eddy simulation (ILES) for a specific frequency. Based on the results of parametric studies for a single strip, several arrangements of multiple strips are considered, and their effects are examined. In addition, the potential capability of using thermal strips to control the amplification of boundary-layer instability and the transition onset is discussed, by evaluating N-factor envelopes.

# 2. Method of analysis

# 2.1. Linear stability analysis

Typically, a spatial LST is employed to interpret the spatial evolution of a disturbance wave in the initial stages of the laminar-turbulent transition. It is well known that a linearly amplified disturbance wave eventually leads to a natural transition of boundary layer; therefore, the result obtained from LST can provide essential insights into the prediction of the transition locus. This study performs a two-dimensional spatial LST analysis for the hypersonic laminar boundary-layer. For the LST analysis, instantaneous flow variables  $\phi = [\rho, u, v, w, T]^T$  are decomposed into the mean and fluctuation components, as follows:

$$\phi = \overline{\phi} + \widehat{\phi}(y)e^{i(\alpha x + \beta z - \omega t)}. \tag{1}$$

Here,  $\overline{\phi}$  is the steady mean flow,  $\widehat{\phi}$  is the disturbance amplitude, and  $\alpha$ ,  $\beta$ , and  $\omega$  denote the streamwise and spanwise wavenumbers and the angular frequency of disturbance, respectively. LST equation can be derived by substituting the expression for flow variables of Eq. (1) into the Navier-Stokes equation, neglecting the nonlinear terms of disturbances based on the small disturbance assumption, and applying a local parallel flow approximation for the mean flow. Because the nonlinear interactions among disturbances are neglected owing to the small disturbance assumption, the LST is valid for predicting the linear growth of an individual disturbance which is usually observed in the early stage of a natural transition of boundary layer. The LST used in the present study was developed by Park and Park [11], in which the analysis method was validated for the case of the Mach 4.5 flat-plate boundary-layer studied by Fedorov and Tumin [12].

Mack's second mode is known as the dominant instability mechanism in two-dimensional and axisymmetric boundary-layers at hypersonic Mach numbers, and a two-dimensional disturbance is known to be the most unstable [13]. Thus, only two-dimensional disturbance waves, where the spanwise wavenumber  $\beta$  is zero are considered in this study. For the spatial LST analysis, the streamwise wavenumber  $\alpha$  is set as an unknown eigenvalue of a complex number:

$$\alpha = \alpha_r + i\alpha_i,\tag{2}$$

where  $\alpha_r$  and  $\alpha_i$  are related to the phase speed and amplification rate of a disturbance wave, respectively. The local instability is determined by the spatial amplification-rate, which is defined as  $-\alpha_i$ . The positive amplification rate represents the growth of the amplitude of the wave as it propagates downstream, corresponding to the destabilization of the boundary layer.

The overall amplification of a disturbance is characterized by the Nfactor:

$$N(x,\omega) = -\int_{x_0}^{x_1} \alpha_i(x,\omega) dx,$$
 (3)

where  $x_0$  is the initial streamwise location, generally chosen as the first neutral point or determined from the receptivity procedure. In this study, the initial point is chosen to be the neutral point of the lower branch of the second mode for each frequency. Note that the N-factor is computed only for the unstable region of Mack's second mode. The first mode that could be identified in the upstream region is not taken into account in the calculation of the N-factor. The N-factor can be used for semi-empirical prediction of the transition onset location based on the  $e^{\rm N}$ -method with a known critical N-factor [14]. Although the  $e^{\rm N}$ -method has been proven practically useful and reliable for predicting the transition location of low-speed boundary-layers with appropriate correlations of the critical N-factor with experimental data, many recent studies also have shown that this method can be applied to hypersonic flows [15, 16]

The steady mean flow data are required for the LST analysis. The commercial computational fluid dynamics software, ANSYS Fluent, is used to compute the mean flow. A density-based solver with a perfect gas assumption is chosen, and specific heat is assumed to be constant,  $c_p = 1006.43 \, \text{J/kg·K}$ . The dynamic viscosity ( $\mu$ ) is determined by the three-

**Table 1**Reference values for non-dimensionalization.

Variable	Reference value
Velocity	${U^*}_{\mathrm{ref}} = {U^*}_{\infty}$
Pressure	${P^*}_{\mathrm{ref}} = {P^*}_{\infty}$
Length	$L^*_{\text{ref}} = 5.0 \text{ m}$
Temperature	$T^*_{\text{ref}} = T^*_{\infty}$
Amplification rate	$\alpha *_{\text{ref}} = 1/\delta *_{x} = (\rho *_{\infty}U *_{\infty}/\mu *_{\infty}x *)^{1/2}$

coefficient model of the Sutherland law. The mean flow variables are non-dimensionalized using the reference values summarized in Table 1. Here, the superscript \* denotes dimensional variables, and the subscripts ref and  $\infty$  denote the reference value and freestream value, respectively. The temperature of the localized thermal strip is non-dimensionalized by the freestream temperature  $(T^*_\infty)$ . The local boundary-layer length scale  $(\mathcal{S}^*_x)$  is used to normalize the amplification rate at each streamwise location.

The computational domain and grid used for the mean flow calculation are depicted in Fig. 1. The streamwise extent and height of the domain are L=1.26 and h=0.4, respectively. The domain is extended to x=-0.06 and x=1.2 from the leading edge to upstream and downstream, respectively. The inlet boundary is set to be located at x=-0.06 to prevent any numerical problem possibly occurring at the leading edge. The grid is constructed with  $2201\times191$  nodes clustered at the wall and leading edge. The grid is clustered so that more than 100 grid points are distributed within the boundary layer to ensure sufficient resolution. A pressure far-field boundary condition with freestream conditions is imposed on the inlet boundary, and a pressure outlet boundary condition is applied to the top and outlet boundaries. For bottom boundaries, no-slip and isothermal boundary conditions are applied to the plate wall (x>0), and a symmetry condition is imposed upstream of the leading edge (x<0).

#### 2.2. Implicit large eddy simulation

Recently, studies that use high-fidelity numerical simulations such as DNS [5,7,8,17] or large eddy simulation (LES) [18-20], to investigate the instability and transition of hypersonic flows, are increasing. Although the LES is cost-effective compared to DNS [20], its result is dependent on grid resolution and the sub-grid scale (SGS) model employed. This shortcoming is more pronounced when resolving the details of the unsteady flow structure near the solid surface is of main interest (e.g. simulation of propagation of instability waves of small amplitude inside the boundary layers). Unlike the LES, which is widely used for a practical analysis of unsteady complex flow, the ILES provides a no-model approach, assuming that a numerical non-linear truncation error of a discretization scheme can describe an implicit SGS model [21]. Therefore, the ILES does not require an explicit SGS model. Instead, an adaptive local deconvolution method based on non-linear truncation errors simulates complex flow phenomena, such as shock and fluid-structure interaction. Thus, the governing equation employed in the ILES is identical to that of the well-resolved DNS, and it corresponds to an under-resolved DNS or pseudo-direct simulation [22]. Several previous studies confirmed the validity of the ILES for the prediction of the hypersonic boundary-layer transition [23,24].

In this study, the ILES is employed to simulate the linear amplification of the disturbance in the hypersonic boundary-layer. A twodimensional ILES is conducted using the open-source finite-difference solver CFDWARP [25], which has been validated against several canonical compressible flow cases. The growth rate computed using the LST is validated by comparing it to the results of the two-dimensional ILES. A combination of the Roe flux differencing scheme [26] and a monotonic upstream-centered scheme for conservation laws (MUSCL) approach [27] was used for the convective flux discretization. The primitive variables that comprise the intercell flux vector were calculated using adaptive seventh/third order weighted essentially non-oscillatory (WENO) interpolation suggested by Balsara et al. [28]

As shown in Fig. 2, the computational domain for the ILES is constructed for the x = 0.2 - 0.7 and y = 0 - 0.0073 regions, where the streamwise extent is determined so that it includes an unstable region of Mack's second mode of the specific frequency of interest. The domain grid has  $4400 \times 170$  nodes clustered at the surface of the flat plate. More than 100 grids are distributed within the boundary layer to ensure sufficient resolution, and at least 20 grids are included within one wavelength of an instability wave of interest. The grid resolution in transverse and streamwise directions used in this study is almost same and approximately half of that used in the DNS studies, respectively. An unsteady disturbance of a specific frequency is imposed at the inlet (x =0.2) using eigenvector profiles obtained from the spatial LST calculation. The initial amplitude of the disturbance is assumed to be 0.5% of the freestream velocity to examine the linear growth of the instability wave. Based on the result of the ILES, the amplification rate of the disturbance is computed as follows:

$$-\alpha_i = \frac{\delta_x^*}{|\phi'|} \frac{d|\phi'|}{dx^*},\tag{4}$$

where  $\phi'$  is the amplitude of a specific component of disturbance wave in the boundary layer. In this study, it is determined based on the maximum amplitude of the streamwise velocity component, which is extracted for the specified frequency via a fast Fourier transform.

#### 2.3. Problem description

The same flow conditions studied by Fedorov and Tumin [12] are considered. The freestream conditions of the mean flow are  $M_{\infty}=4.5$ ,  $T^*_{\infty}=61.11$  K,  $P^*_{\infty}=1008.64$  Pa, and  $Re_{unit}=1.0\times10^7$  m $^{-1}$ . The flat-plate boundary-layer with adiabatic wall condition without any strip is designated as a baseline case for comparison. To evaluate the influence of local heating/cooling strips, the boundary layers over a single strip of various streamwise locations, lengths, and heating/cooling intensities are considered. Several combinations of strips in the sequential arrangement are also investigated for the same freestream conditions. Except for the strip section, the plate surface is assumed to be an isothermal wall at  $T^*_{\rm w}=272$  K, which corresponds to the adiabatic wall temperature ( $T^*_{\rm ad}$ ).

The evolution of an instability wave of a specific frequency is investigated for the various single/series of strip configurations. A normal(discrete) mode of two-dimensional disturbance (i.e., Mack second mode instability) with a non-dimensional frequency of F=50 is chosen for both validation and parametric studies. The non-dimensional frequency (F) is defined as follows:

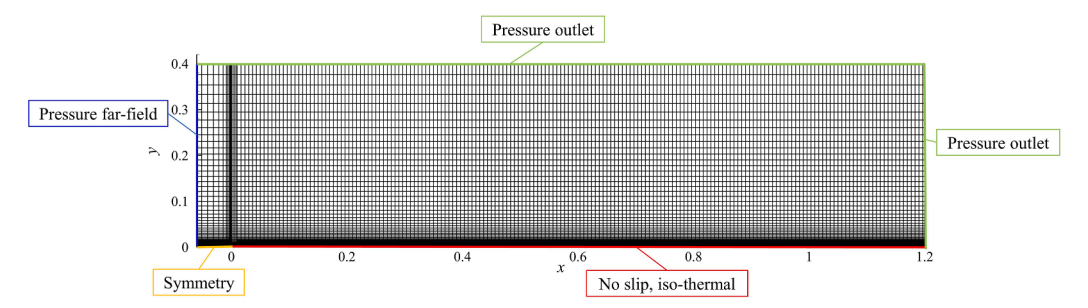


Fig. 1. Computational grid for mean flow (Fluent).

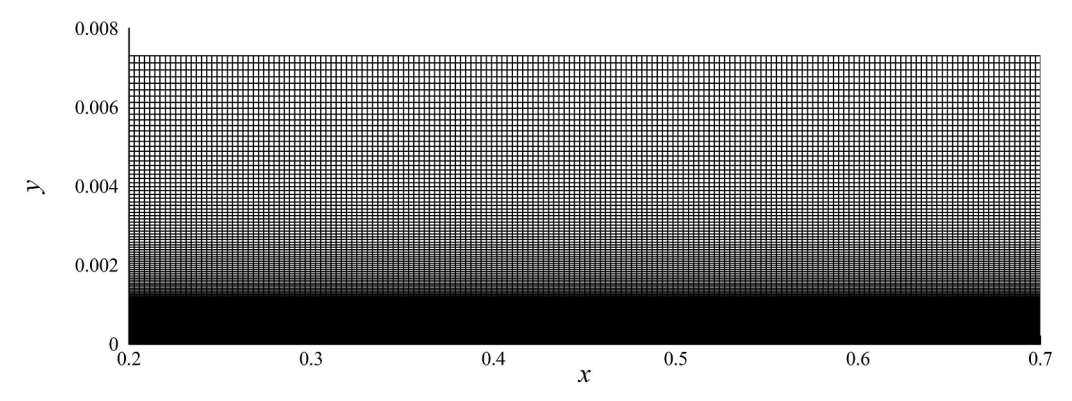


Fig. 2. Computational grid to analyze instability of disturbance (ILES).

$$F = \frac{2\pi f^* \nu_{\infty}^*}{\left(U_{\infty}^*\right)^2} \times 10^6,\tag{5}$$

where  $f^*$  and  $\nu_\infty^*$  denote the dimensional frequency and kinematic viscosity of the freestream, respectively. In addition to the basic parameter studies for the single frequency, the overall effects of the strip are investigated by carrying out analyses for various frequencies in the range of F=30-150. The influences of the strips on the amplification of second-mode instability are evaluated by comparing the results with the baseline case.

Temperature distribution on the thermal strip, considered in this study, is schematically shown in Fig. 3. The temperature varies smoothly along the streamwise direction with the maximum/minimum temperature at the midpoint of the strip. The distribution is designed to be similar in shape to the Walker and Greening symmetric hump geometry used in previous studies [11,29,30]. The temperature distribution along the strip is defined using Eq. (6):

$$T_s = T_w + (T_c - T_w) \cdot f(t)$$
(6)

where  $t = (x - x_c)/b$ ,

$$f(t) \, = \, \left\{ \begin{array}{ll} 1 - 3t^2 + 2|t|^3, & \text{if} \, |t| \leq 1 \\ 0, & \text{if} \, |t| > 1 \end{array} \right. .$$

The temperature distribution along the strip  $(T_s)$  is a function of the temperature at the center of the strip  $(T_c)$ , the half-width of the strip (b), and the distance from the strip center  $(x - x_c)$ . The continuity of the temperature along the streamwise direction is ensured because the wall temperature  $(T_w)$  is assumed along the wall other than the strip regions.

The configurations of the local thermal strips considered in the present study are summarized in Table 2. The baseline case without a strip is used as a reference for evaluating the effects of local temperature variations. Three strip lengths, represented as L1, L2, and L3, are

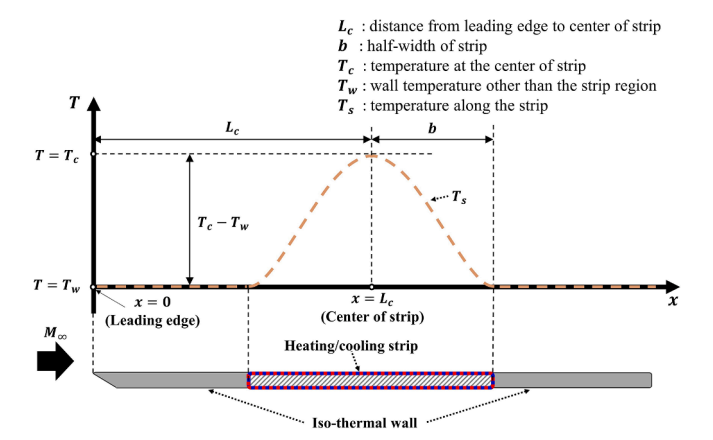


Fig. 3. Schematic of temperature distribution along surface.

**Table 2**Cases of local heating/cooling strip.

Case	Location $(x_c)$	Length $(L_s)$	$T_{\rm c}/T_{\rm w}$	Info.
baseline	-	-	1.0	Isothermal wall
x1-H1-L1	0.28	5λ	1.4	Single
x1-H1-L2	0.28	$10\lambda$	1.4	strip
x1-H1-L3	0.28	20λ	1.4	
x2-H1-L3	0.33	20λ	1.4	
x3-H1-L3	0.38	20λ	1.4	
x1-H2-L2	0.28	$10\lambda$	1.6	
x1-C1-L2	0.28	10λ	0.6	
x1-C1-L3	0.28	20λ	0.6	
x1-C2-L2	0.28	$10\lambda$	0.4	
combination A	0.28, 0.33,	20λ	0.6, 0.6,	Combination of
	0.38		1.4	strips
combination B	0.28, 0.33,	20λ	1.4, 1.4,	
	0.38		0.6	

examined. The strip length is determined based on a wavelength ( $\lambda$ ) of a disturbance wave of frequency F=50 propagating at freestream speed. The wavelength is computed as follows:

$$\lambda = \frac{U_{\infty}^*}{f^* I^*}.\tag{7}$$

It has to be noted that the actual phase speed of the instability wave is different from the freestream speed. The actual phase speed would be the phase speed of mode S in the region of interest and it is approximately the speed corresponding to the range, where the relative Mach number is subsonic. It is not significantly different from the freestream speed, and the difference is smaller than the speed of sound compared to the freestream speed. Moreover, the actual phase speed of mode S varies with the streamwise location; not desirable for use as a fixed reference length scale. Therefore, for convenience, the wavelength of the artificial wave at a phase speed of freestream speed is chosen as the base length scale and is  $\lambda = 0.002$  for F = 50. The strip length for the cases of L1, L2, and L3 is set as  $5\lambda$ ,  $10\lambda$ , and  $20\lambda$ , respectively. The locations of the strip center, which are denoted as x1, x2, and x3, are chosen based on the gradient of the amplification rate  $(-d\alpha_i/dx)$  of F = 50 for the baseline case. The x1, x2, and x3 are determined as  $x_c = 0.28$ , 0.33, and 0.38, and they are corresponding to the location of positive, nearly zero, and negative values of the gradient of the amplification rate, respectively. According to a previous study [11], the synchronization point, where mode F and mode S for F = 50 are synchronized, is located at x = 0.2906. Therefore, x1 is the location relatively upstream from the synchronization point, and x2 and x3 are downstream locations from it. The influence of the heating/cooling strength  $(T_c/T_w)$  is also investigated for several cases of heating (H1, H2) and cooling (C1, C2). The heating/cooling intensities of H1, H2, C1, and C2 are set to be  $T_c/T_w = 1.4$ , 1.6, 0.6, and 0.4, respectively.

#### 3. Results and discussion

#### 3.1. Validation

The methods of mean flow calculation and stability analysis were validated for the baseline case. The mean flow data computed by using Fluent are compared with a similarity solution of the compressible boundary-layer equation obtained by using the method described in Ref. [31]. As shown in Fig. 4a, at x=0.3, the velocity and temperature profiles are in good agreement with each other. The boundary-layer thickness  $\delta$ , defined as  $u(\delta)=0.95$ , is depicted in Fig. 4b. There is no notable difference between the results from the two different methods.

The analyses were carried out by using both the spatial LST and ILES for a disturbance of F = 50, and the resulting local amplification rates are compared in Fig. 5a. By keeping in mind that the stability results are very sensitive to the mean flow and analysis method employed, the amplification rates can be judged to be in reasonable agreement, although there are discernible discrepancies. One of the possible reasons for the difference, which is more pronounced in the upstream region, can be attributed to the non-parallel effect, which is not taken into account in the LST analysis. In general, the non-parallel effect isknown to make the boundary layer more unstable in the upstream region. It has been observed from previous studies that the amplification rate obtained from DNS is greater than that of LST near the upstream regions [32–36]. However, in this study, the amplification rate of LST is found to be greater than that obtained from ILES. Further investigations of the results confirm that there is a region of transient behavior in ILES, for which the imposed profiles of mean flow (similarity solution) and instability wave (eigensolution of LST) at the inflow boundary are gradually settled down and eventually adjusted to the solution of the Navier-Stokes equations. The adjustment of solution is expected to be the main origin of the discrepancies in the amplification rate observed in the upstream region. Considering these aspects of ILES, it can be concluded that the LST analysis provides fairly good results reflecting essential physics and are sufficient for the parametric study of qualitative changes. A comparison of N-factor curves is shown in Fig. 5b. The overall tendencies of the LST results are in good agreement with those from ILES for the linear amplification of the second mode instability, and the validity of the method of analysis is confirmed.

# 3.2. Parametric study on a single strip

A parametric study on a single strip is conducted for a discrete instability wave of F=50. The effect of the three parameters described above (temperature intensity, location, and length) are investigated. The mean flow data is obtained by using Fluent, and the amplification rate at each streamwise location is computed via LST analysis.

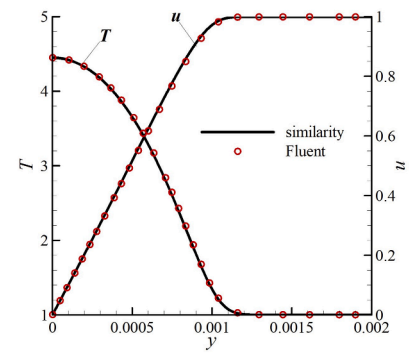
#### 3.2.1. Temperature intensity

The influence of the strip intensities is examined for fixed location and length of  $x_c = 0.28$  (= x1) and  $L_s = 10\lambda$  (= L2), respectively. Fig. 6 shows the pressure contours around the heating/cooling strip. Two types of pressure waves are identified around the strip; one is a compression wave, and the other is an expansion wave. For the heating strip, a compression wave is formed in the vicinity of the leading edge, and an expansion wave is formed around its end. On the contrary, the order of the pressure waves is reversed in the cooling-strip case. The compression wave is induced when the wall temperature changes from relatively low- to high temperature (positive gradient), whereas an expansion wave is formed when the wall temperature changes from relatively high- to low temperature (negative gradient). This characteristic is identical to the result observed in the previous studies on a local single heating/cooling strip [5,7,8].

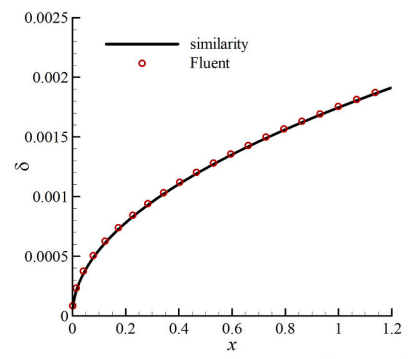
This phenomenon can also be observed from the resulting surface pressure distribution, as depicted in Fig. 7a. The strength of the pressure wave is proportional to the temperature intensity( $|T_c - T_w|$ ), and the preceding pressure wave exhibits a pressure variation greater than the following one. It is easily seen from Fig. 7a that the compression wave and the expansion wave are induced near the region of the positive and negative temperature gradient, respectively. The streamwise variation of boundary-layer thickness ( $\delta$ ) is plotted in Fig. 7b. The boundary-layer thickness around the heating strip is found to be greater than that of the baseline case, and the behavior is opposite for the cooling strip. From the viewpoint of the pressure wave, the boundary-layer thickness increases through the compression wave and decreases through the expansion wave. It is noteworthy that these characteristics of the mean flow are similar to those around a smooth hump [11,17,37–39]. According to the comparison of the mean flow, the heating strip is expected to have an impact on the boundary-layer instability, which is analogous to a smooth hump.

The LST results of the amplification rate ( $-\alpha_i$ ) and N-factor for various temperature intensities are compared in Fig. 8, together with those of the baseline. As depicted in Fig. 8a, the strip leads to both unstable and stable effects on Mack's second-mode instability. Compared to the baseline case, the instability wave undergoes an abrupt increase in the amplification rate (i.e., makes the boundary layer unstable) in the vicinity of the compression-wave region. Contrarily, a sharp decrease in the amplification rate is observed through the region of the expansion wave. Although the strip possesses both stable and unstable regions around it, the destabilization is more significant than that of the stabilization for the cases of the heating strips, whereas the cooling strips exhibit the opposite tendency. This is consistent with the observation that the strength of the preceding pressure wave is stronger than the following pressure wave.

The corresponding N-factor curves are depicted in Fig. 8b, and the total influence of the strip is evaluated. There are noticeable differences between the presence of strips and baseline cases. As expected from the



(a) Streamwise velocity/temperature profile



(b) Boundary-layer thickness ( $u(\delta) = 0.95$ )

Fig. 4. Comparisons of mean flow profiles at x = 0.3 and distribution of boundary-layer thickness.

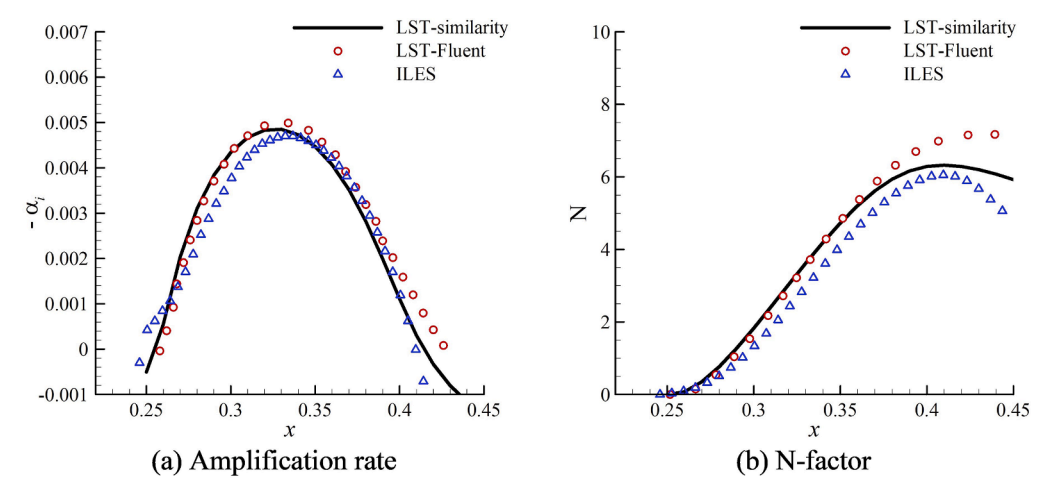


**Fig. 5.** Comparisons of stability analysis results for baseline case (F = 50).

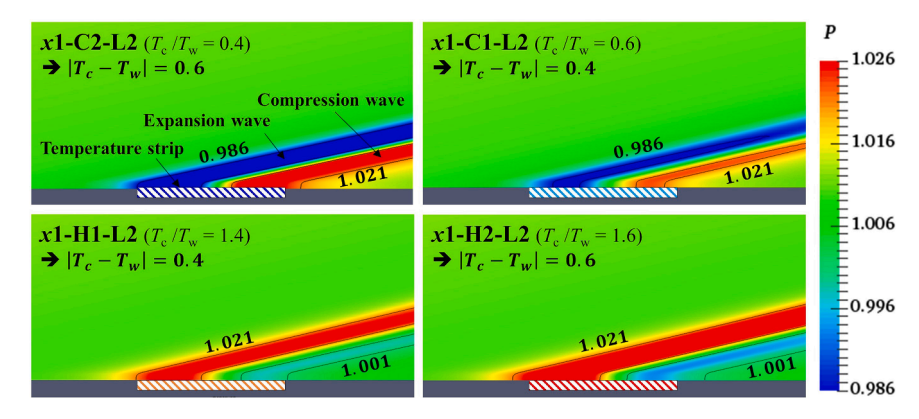


**Fig. 6.** Pressure contours around a single local strip ( $x_c = 0.28, L_s = 10\lambda$ ).

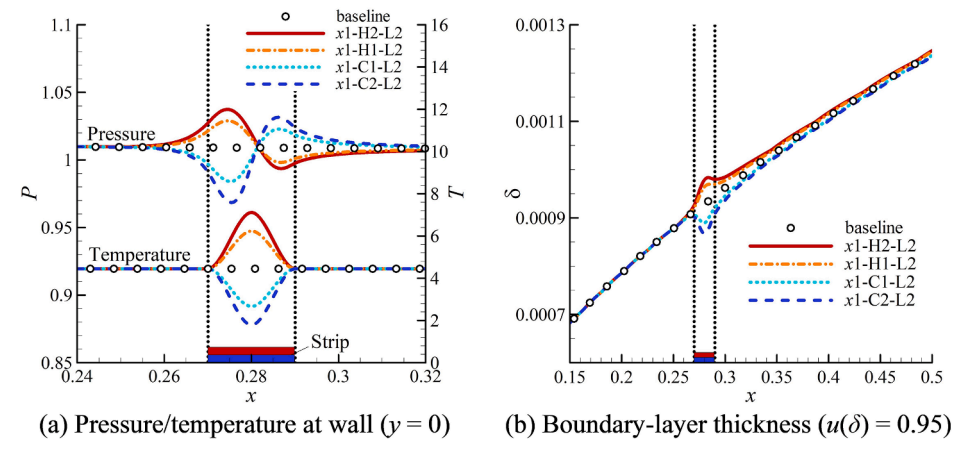
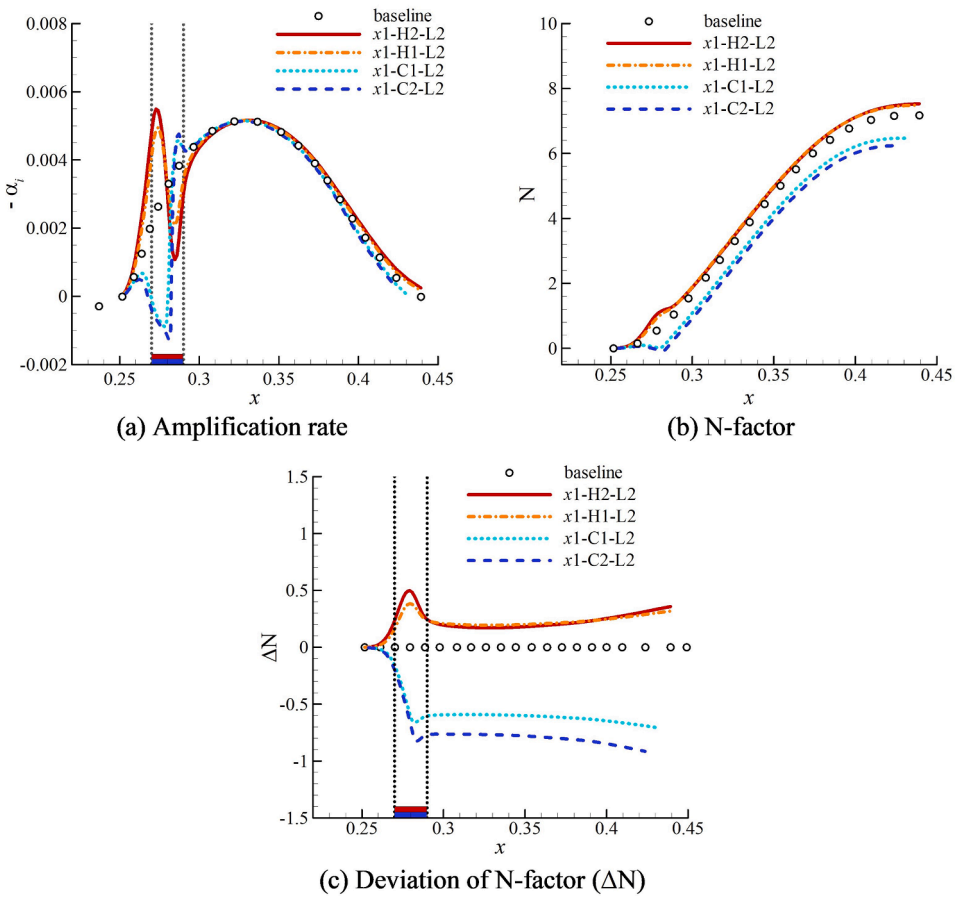


Fig. 7. Comparisons of mean flow for different temperature intensities.

amplification rate results, the heating strips cause a destabilization effect, and the cooling strips lead to a stabilization effect. Quantitatively, the amount of the overall stabilization effect of the cooling strip is greater than that of the destabilization effect of heating strips. As seen in Fig. 7a, the deviations of surface pressure induced by the cooling strips are greater than that by the heating strips, and this difference in pressure deviation is expected to be the reason for the difference in the overall stabilization/destabilization of Mack's second-mode instability. The deviation of N-factor from the baseline case, which corresponds to  $\Delta N$  (=N(x) – N<sub>baseline</sub>(x)), is compared in Fig. 8c. The local peak value of  $\Delta N$ 

in the vicinity of the thermal strip for the cases of x1-C1-L2 and x1-H1-L2 are  $\Delta N_{peak}=-$  0.66 and 0.38, respectively. Thus, in terms of  $\Delta N_{peak}$ , the stabilizing effect of the cooling strip is almost double the destabilizing effect of the heating strip for the same deviation of temperature. As the thermal intensity increases, the pressure waves around the strip intensity, and thus the corresponding overall stabilization/destabilization impact on the second-mode instability is strengthened. However, the changes in the N-factor with respect to heating/cooling intensity are found to be relatively small. The difference of  $\Delta N_{peak}$  is only approximately 0.11 between the two heating strip cases (i.e., x1-H1-L2 and x1-



**Fig. 8.** Comparisons of stability analysis results for temperature intensity (F = 50).

H2-L2). The corresponding value for the cooling strip cases is approximately 0.16. Thus, it can be deduced from the results that the pressure wave induced by the streamwise temperature gradient is the major factor by which the thermal strip affects the hypersonic boundary-layer instability.

It is easy to expect that the deviation of N-factor must remain constant where the presence of the thermal strip no longer affects the mean flow, i.e., the mean flow completely recovers to that of the baseline case. Naturally, the same mean flow yields the same growth rate, so the N-factor will change by the same amount, keeping the N-factor deviation at the same value. However, the results in Fig. 8c show that the N-factor deviation does not converge to a constant value downstream and still changes even in the vicinity of  $x \approx 0.45$ . This result confirms that the mean flow around x = 0.45 is still different from the baseline case and is discernible enough to result in a different growth rate in LST analysis.

We note that Fig. 8 presents the results of calculations carried out only up to the second neutral point (i.e., only unstable region) for all cases. While keeping in mind that the streamwise extent of the computational domain is up to x = 1.2 (see Fig. 1), the mean flow and resulting growth rates were evaluated further in detail beyond the second neutral point. Although not shown here, in terms of resulting growth rates, it is identified that the influence of the thermal strip on mean flow remains even further downstream and that the mean flow does not completely recover to the baseline case up to the end of the computational domain. Beyond the second neutral point, however, the discrete mode of our interest enters a stable region so that the growth rate becomes a negative value and the N-factor starts to decrease (see Fig. 8a and 8b). By analyzing the data downstream of the second neutral point, it is revealed that the instability becomes less stable and more stable in the heating and cooling strip cases, respectively compared to the baseline case (Fig. 8a and 8c). Although the effect of the thermal strip on both mean

flow and stability results appears along a very long streamwise extent, we hereafter mainly focus on analyzing the results for the unstable region because a stable region is expected not to contribute to the occurrence of the transition. From the viewpoint of amplification of instability wave and transition, the further increase in the N-factor deviation beyond the second neutral point can be regarded as a less-meaningful feature because the N-factor itself will decrease (Fig. 8b).

# 3.2.2. Length

The impact of the heating strip length is examined for several lengths:  $5\lambda$  (= L1),  $10\lambda$  (= L2), and  $20\lambda$  (= L3). The wall pressure and the boundary-layer thickness along the streamwise direction are plotted in Fig. 9. The streamwise extents for the cases of L1, L2, and L3 are marked with a solid, dotted, and dashed line, respectively. The results of Fig. 9a show that the longer heating strip causes milder temperature and pressure gradients, and the distance between the strip center and the location of maximum pressure deviation also increases. As the distance between the strip center and the pressure-peak location increases, the pressure gradient at the strip center is reduced. Since Eq. (6) is used, a longer strip induces a smaller temperature gradient along the streamwise direction, and this feature results in gradual pressure changes in longer streamwise extents for the mean flow. The pressure gradient near the leading edge of the strip is greater than that at the end, regardless of the strip length. Fig. 9b shows the distribution of boundary-layer thickness for three strip lengths. As the strip length increases, the maximum boundary-layer thickness increases. While the temperature distribution is symmetric with respect to the strip center, the location of the maximum deviation of boundary-layer thickness is formed slightly downstream from the strip center. As the strip length increases, the adverse pressure gradient and subsequent favorable pressure gradients weaken, and the pressure wave develops along the longer streamwise

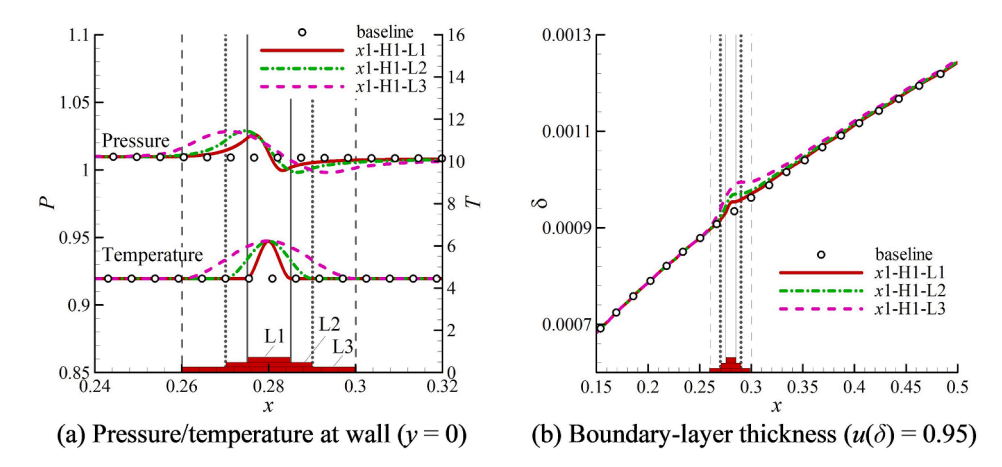


Fig. 9. Comparison of mean flow for different strip lengths.

extent. These weak pressure gradients over a longer distance make the location of the peak deviation of boundary-layer thickness move further downstream.

Fig. 10 shows the corresponding results of the stability analysis for three strip cases. As shown in Fig. 10a, as the heating strip's length increases, a deviation of the amplification rate from the baseline case is observed in a broader region, and the local peak around the strip decreases. The deviation of the amplification rate has a trend similar to the pressure distribution along the streamwise direction (see Fig. 9a). The changes in the amplification rate with respect to the strip length are more considerable in the region around the leading edge than the aft region of the strip. The overall destabilization effect of the heating strip

is found to be more significant for the long strip as can be seen from Fig. 10b and 10c. In Fig. 10c, the deviation of N-factor ( $\Delta$ N) is compared for different strip lengths. The longer strip exhibits a larger N-factor increment, and the case of the longest strip (x1-H1-L3) has the greatest local peak value ( $\Delta$ N<sub>peak</sub>) of 0.6. Thus, a long thermal strip has a more significant influence on the second mode instability. As discussed in the previous section, the deviation of the N-factor is still increasing even in the vicinity of the second neutral point ( $x \approx 0.45$ ). The longer the strip length, the greater the changes in the N-factor deviation. It seems natural because as strip length increases, the influence of the strip on the change in the mean flow downstream would become stronger. As mentioned before, however, the continuous changes in the N-factor

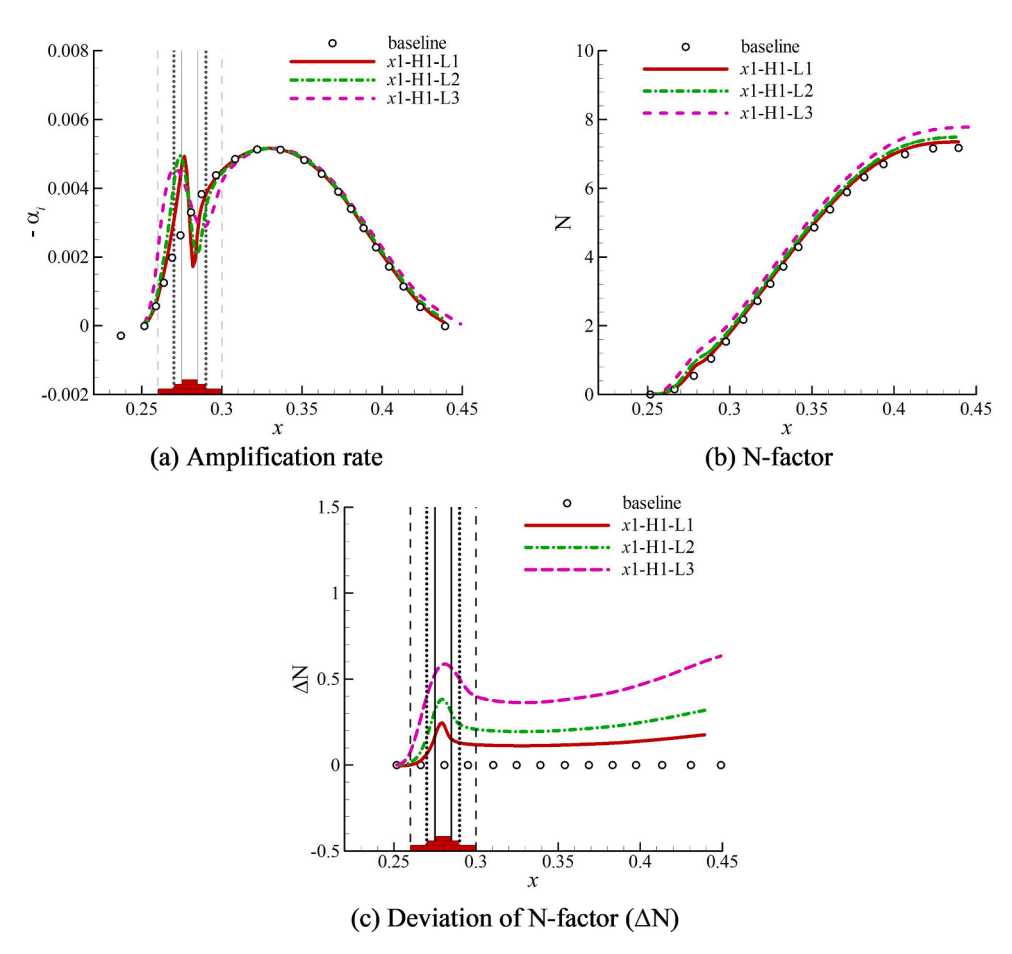


Fig. 10. Comparison of stability analysis results for different strip length (F = 50).

deviation within the stable region (i.e., beyond the second neutral point) is not a main concern of the present study.

#### 3.2.3. Location

For a fixed intensity and length (H1-L3), a strip at three different locations (i.e., x1, x2, and x3) is examined, and the corresponding results of mean flow are shown in Fig. 11. As discussed earlier, wall temperature variation induces compression waves in the vicinity of the leading edge, which makes the wall pressure and boundary-layer thickness increase around the upstream of the strip center. Similarly, the negative temperature gradient beyond the strip center results in a generation of expansion waves and a decrease in the deviation of boundary-layer thickness. As can be seen in Fig. 11a and 11b, no notable difference in the mean flow is identified depending on the location; the variations in the wall pressure and boundary-layer thickness possess similar trends to those mentioned in the previous sections.

The results of the stability analysis for three locations are depicted in Fig. 12. There are noticeable differences in the amplification rate depending on the strip location (Fig. 12a). As consistent with the observation made in the preceding sections, in the case of location x1, the relatively strong upstream compression destabilizes the hypersonic boundary-layer, and the subsequent weak expansion yields stabilizing effects. On the other hand, in the case of the strip at x2, the influences of the streamwise compression and expansion on change in the growth rate are rather reduced. Moreover, in the case of the strip at x3, reversed effects appear for the same sequential pressure variation. In the vicinity of x3, the compression upstream of the strip stabilizes the instability wave, and the following expansion makes it unstable.

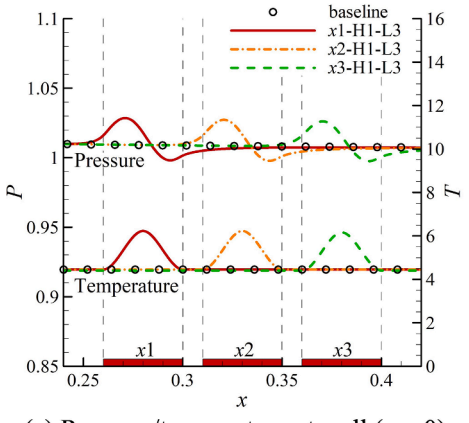
To validate this reversed effect and ensure whether the LST analysis captures the essential physics properly, the ILES computation is carried out for the two extreme cases (x1-H1-L3 and x3-H1-L3). As plotted together in Fig. 12a and 12c, the amplification rate computed by the ILES exhibits similar qualitative trends compared to that of LST. This allows us to conjecture that the effect of the streamwise pressure gradient is reversed in the region where the streamwise gradient of the amplification rate is negative for the baseline case (i.e., the case of no strip). This implies that the heating strips can provide different influences on the second-mode instability depending on its location, even though the changes in mean flow owing to the strip are subject to similar characteristics. The N-factor and its deviation obtained from the LST and ILES calculation are shown in Fig. 12d and 12e. From these results, it is confirmed again that the opposite influence emerges depending on the strip location. In the case of x1-H1-L3, the boundary-layer is locally destabilized by  $\Delta N_{LST,\ peak}=0.59$  and  $\Delta N_{ILES,\ peak}=0.53,$  whereas the x3-H1-L3 case produces the stabilization corresponding to  $\Delta N_{LST, peak} =$ -0.28 and  $\Delta N_{ILES, peak} = -0.38$ . In Fig. 12e, the case of x2-H1-L3 shows both stabilization and destabilization of the second mode instability.

From these results, it is expected that the critical point where the effect of the thermal strip is reversed is located between x2 and x3. Although not shown here, through the results of additional calculations, the same reversal phenomenon was also confirmed for the cooling strip. Further downstream around and beyond the second neutral point, all the heating strip cases exhibit a less stable tendency than the baseline case, as observed before.

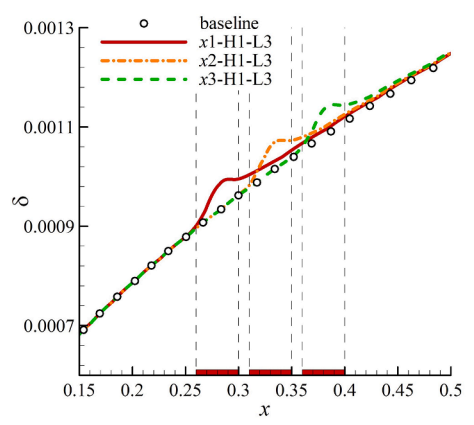
The contour of pressure perturbation from the ILES results is shown in Fig. 13 for the baseline. The amplified pressure fluctuation exceeding a certain amplitude is discernible in the region of 0.35 < x < 0.5. The result shows the entire evolution, i.e., growth and decay, of the disturbance of a specific frequency governed by the instability mechanism. In Fig. 14 and 15, the contours for pressure and temperature disturbances are compared for the cases of baseline, x1-H1-L3, and x3-H1-L3. The pressure disturbance along the wall-normal direction has a two peaks structure with a larger magnitude for the peak close to the wall and a nearly opposite phase between the two peaks (see Fig. 14). In addition, as can be seen in Fig. 15, the rope-like structure in the vicinity of the boundary-layer edge appears in the temperature disturbances. These features of the perturbation structure are typical characteristics of the second-mode instability and have been reported by many previous studies [7,40]. A comparison represents that the amplitude of pressure perturbation for the case of x1-H1-L3 becomes greater than that for the baseline case (see Fig. 14a and 14b), while it has been suppressed for the case of x3-H1-L3 (see Fig. 14c). The same tendency is also observed for the temperature perturbation in Fig. 15, which indicates that the effect of the strip is reversed depending on its location relative to a specific threshold point.

The instantaneous pressure perturbation signals along the wall are compared in Fig. 16. The case of x1-H1-L3 attains the largest amplitude, whereas the case of x3-H1-L3 reaches the smallest amplitude (see Fig. 16a). In the case of x3-H1-L3, most of the delay or suppression in the disturbance amplitude is found to occur in the region over the strip; thus, the amplitude is smaller than that of the baseline case. This observation indicates that the compression in the streamwise direction (adverse pressure gradient), owing to the presence of the strip yields a stabilization effect for this case. After this stabilization region, a slight destabilization effect related to the streamwise expansion follows and it stimulates the growth of perturbation, which makes the amplitude tends to recover to that of the baseline case. Therefore, the ILES results confirm again that a thermal strip can lead to either a stabilization or destabilization effect, and its effect depends on the strip's location. The results also indicate that the effect of the strip can be reversed as its location moves downstream beyond a certain critical point.

It has been reported that the location of a smooth hump (roughness element) [17,37-39] or porous coating [41,42] relative to the synchronization point is a critical factor that determines the influence on



(a) Pressure/temperature at wall (y = 0)



(b) Boundary-layer thickness ( $u(\delta) = 0.95$ )

Fig. 11. Comparison of mean flow for a strip at different locations.

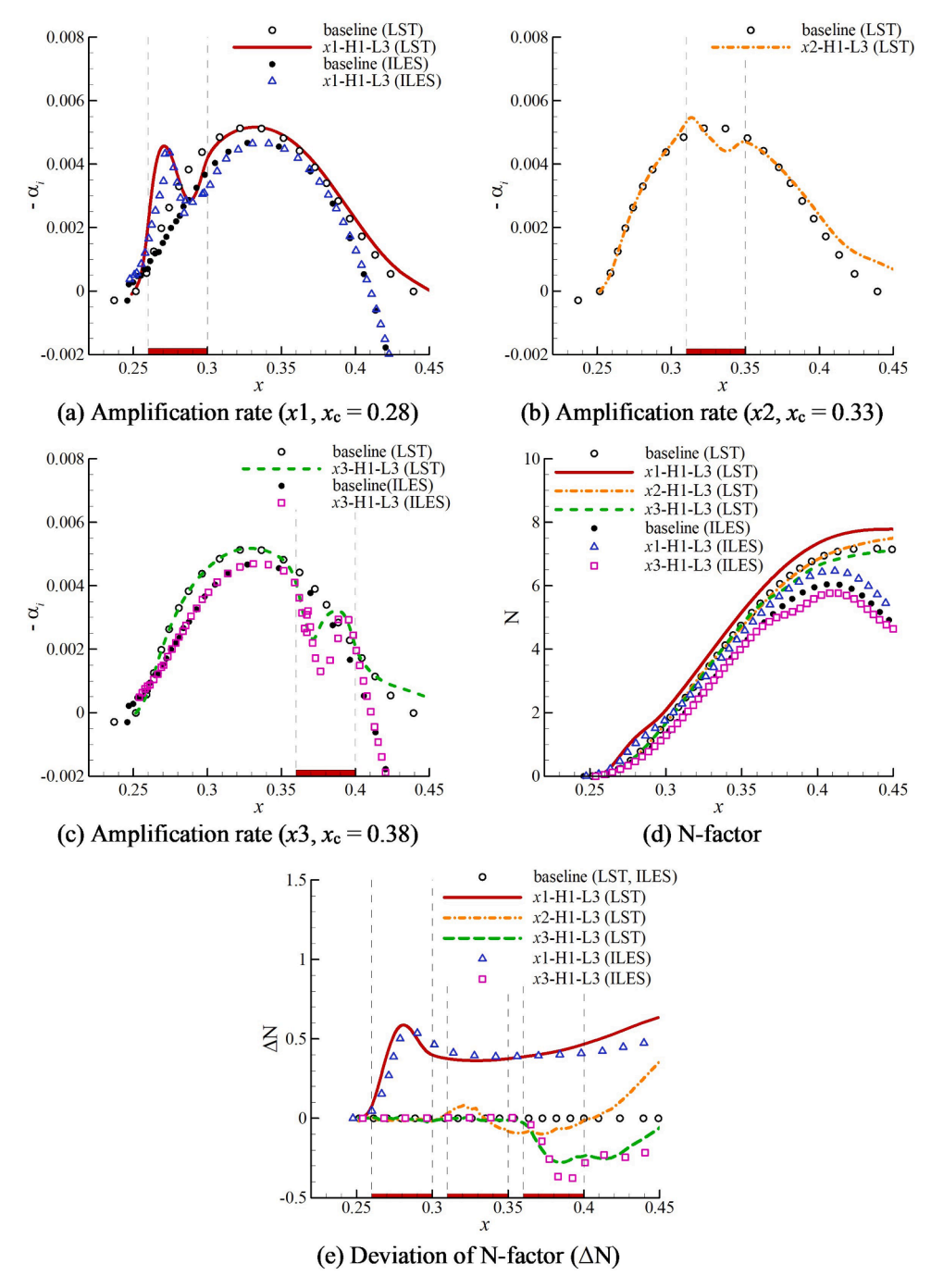
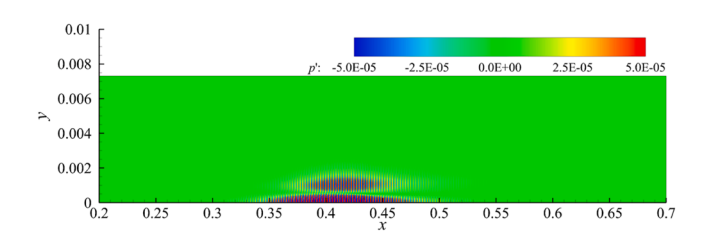


Fig. 12. Comparison of stability analysis results for different locations (F = 50).



**Fig. 13.** Contour of pressure perturbation for the baseline case (F = 50).

Mack's second-mode instability in hypersonic boundary-layers. Zhao et al. [8] also discussed the importance of the relative location of a single local heating/cooling strip to the synchronization point. According to a

study of Park and Park [11], the synchronization point for the baseline case of present consideration is  $x_{\rm sync}\approx 0.29$ . From the parametric study of the strip's location, the threshold or critical point, where the reversal effect emerges, is found to be located between x2 and x3, i.e.,  $0.33 < x_c < 0.38$ . To identify the reversal location of the thermal strip more in detail, several strip locations in the range of  $0.28 < x_c < 0.38$  are additionally computed using the LST. The values of the deviation of N-factor at the second neutral point of the baseline case ( $x_{\rm np}$ ,  $z_{\rm nd} \approx 0.435$ ) are collected and plotted in Fig. 17. The reversal point is found to be  $x_{\rm rev} \sim 0.336$ , and this point is obviously different from the synchronization point. The reversal point ( $x_{\rm rev}$ ) appears to be almost located at the midpoint of two neutral points and located further downstream than the synchronization point. Further investigation reveals that the reversal point is very close to the point where the growth rate of the

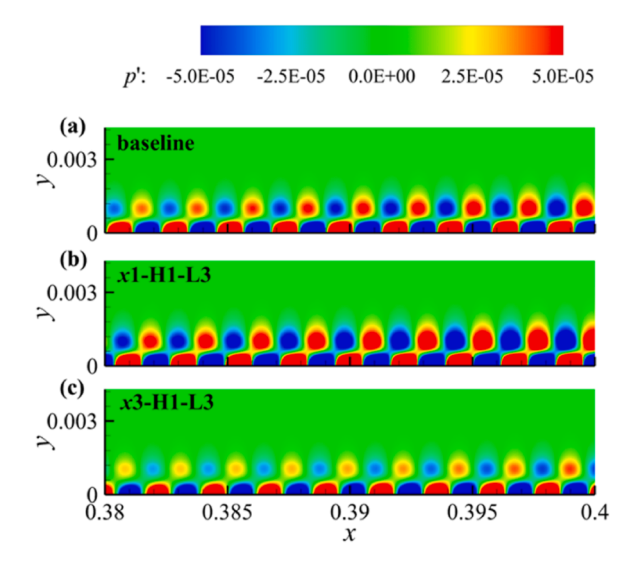


**Fig. 14.** Contours of pressure perturbation (0.38 < x < 0.4).

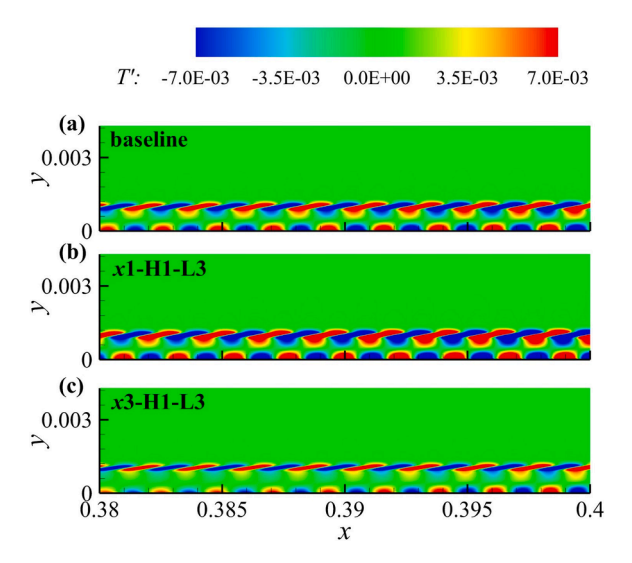


Fig. 15. Contours of temperature perturbation (0.38 < x < 0.4).

second mode becomes maximum ( $x_{\rm gr,\,max} \sim 0.3254$ ) in the baseline case. From the results of the present study which are based on the spatial analysis, the reversal point is identified as in the vicinity of the location of the maximum growth rate, not the synchronization point. This result is somewhat consistent with the observation from the asymptotic analysis with a temporal viewpoint carried out by Zhao and Dong [10]. Thus, the reversal point ( $x_{\rm rev}$ ), where the opposite influence of the thermal strip on the second-mode instability occurs, is located near the maximum growth rate point rather than the synchronization point.

As observed and discussed so far, the reversal point can be characterized by being slightly downstream of the location of the maximum growth rate. Based on the results of the parametric study, the relative location of the wall-temperature induced streamwise compression/expansion to the reversal point is an important factor that determines the strip effect on Mack's second-mode instability.

# 3.3. Applications

# 3.3.1. Combination of thermal strips

Based on the results from the parametric study in the previous section, combinations of the strips, in which three strips are arranged in series, are examined. The same instability wave of F=50 is considered. Two types of combinations, A and B, are designed to maximize the stabilizing and destabilizing effects on the instability wave, respectively. Both combinations comprise three strips with a length of  $20\lambda$  (= L3) and thermal conditions are summarized in Table 2. Combination A consists

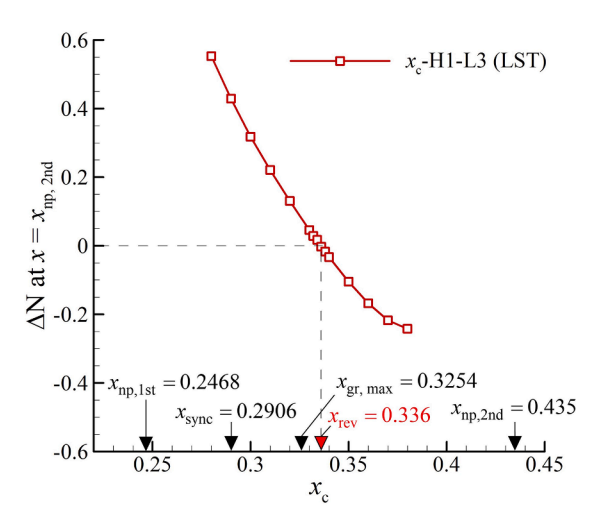


Fig. 17. Deviation of N-factor at second neutral point of baseline case.

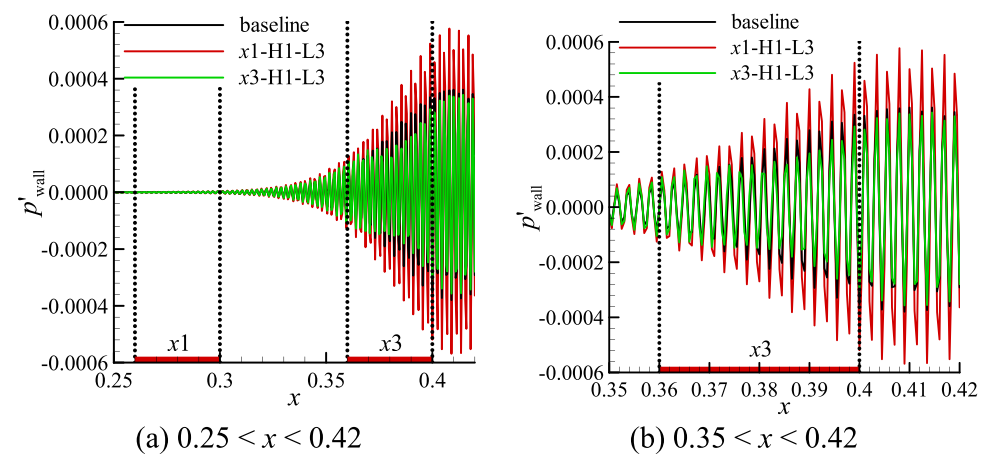


Fig. 16. Comparison of pressure perturbation at wall (y = 0)

of two cooling strips of C1 and one heating strip of H1, in order, while combination B corresponds to the opposite composition.

Comparisons of the resulting mean flow for the two combinations are presented in Fig. 18. The wall pressure distributions appear to be opposite each other while showing the same dependency on the temperature discussed in the previous sections (see Fig. 18a). The streamwise variation of the boundary-layer thickness for each combination (Fig. 18b) shows a considerably different trend on the deviation with respect to the baseline case along streamwise direction. Because the first two strips located at x1 and x2 are the same thermal type and the subsequent strip is a different type, the streamwise compression or expansion is continued and extended in the region between x2 and x3. From the previous section, the effect of the pressure change is found to be reversed just before x3; therefore, these thermal strip arrangements are expected to maximize the influence on the growth of the instability wave.

The stability analyses for the cases of two combinations are carried out, and the resulting amplification rates and N-factor curves are shown in Fig. 19. The ILES computation is also conducted to check the reliability of the LST, and the resulting amplification rates are compared together. As can be seen in Fig. 19a, combination A results in stabilization effects over most of the streamwise extent, as intended. However, a significant deviation between the two analysis methods is identified around the first cooling strip. The adjustment of the solution in the upstream region, discussed before, is considered the underlying reason for the discrepancy between LST and ILES results, and its impact seems to be much more pronounced in this case. Except for this region, the LST prediction still exhibits a similar trend to that of the ILES. Similarly, the overall destabilizing effect of combination B is observed in Fig. 19b, and the LST results exhibit fairly good agreements with the ILES. The results of Fig. 19 indicate that LST can properly predict the overall trends even for the cases of strip combinations.

In the previous section, both LST and ILES predicted well the reversal phenomenon occurring between the locations of the second and third strips. Based on the LST results, the reversal point is  $x_{\rm rev}=0.336$ , located relatively downstream of the synchronization point. Although the streamwise compression is present near the fore region of the third strip, because of the reversal phenomenon, the second mode becomes stable in the region of the third strip for combination A. Similarly, the reversal phenomenon is also observed in the corresponding region for combination B. Thus, the critical point of reversal can be regarded as approximately  $x_{\rm rev}=0.336$  for the flow conditions and instability wave frequency studied. This observation confirms again that the reversal point is different from the synchronization point. We note that this phenomenon has been explored and investigated only for the unstable region of the second-mode instability with F=50.

The N-factor and its deviation from the baseline case ( $\Delta N$ ),

calculated using the amplification rate from LST analysis, are compared in Fig. 19c and 19d. The results reveal that combinations A and B result in stabilization and destabilization effects compared to the baseline case. In terms of boundary-layer transition, it is expected that combination A can lead to a delay of the transition, whereas combination B can lead to early transition onset. This indicates that a designed array of thermal strips might be used as an active control methodology to control the transition location. From the other point of view, a non-uniformity of the wall-temperature distribution possibly causes a change in transition location in an undesirable direction, which eventually can result in the failure or loss of a hypersonic vehicle.

#### 3.3.2. Overall effects

The N-factor curves of various frequencies for the cases with and without the heating/cooling strips are calculated and analyzed to evaluate the overall effects of the strips. Two cases of the single strip and two cases of strip combination are considered for the investigation. The calculations are conducted for frequencies in the range of F=30-150. It should be noted that the N-factor is calculated only for the unstable region of the second mode for each frequency.

The cases of x1-C1-L3 and x1-H1-L3 are selected as representative cases for single-strip analyses, and the resulting N-factor curves are shown in Fig. 20. As shown in Fig. 20a, the N-factor envelope is identical to that of the baseline case in the far upstream. However, the envelope undergoes abrupt deviations in the vicinity of the strip and it increases rapidly in the region of the strip. This sudden destabilization region is caused by N-factor curves corresponding to frequencies suffering the reversal phenomenon. It has to be noted that the location of the critical point of the reversal phenomenon would vary with frequency, while the strip location is fixed. Thus, there are frequencies subjected to the reversal phenomenon for the specified strip location which results in the destabilization region in the N-factor envelope. However, the cooling strip also produces a region of stabilization downstream of the strip. An opposite behavior is observed in the case of the heating strip in Fig. 20b. The stabilizing effect, induced by the reversal phenomenon, occurs over the strip region, followed by a subsequent region of destabilizing effect downstream of the strip. In the region far downstream, it is seen from the Fig. 20 that the cooling and heating strips result in slightly higher and lower values of N-factor for the same frequency, respectively. It has been known from previous studies that entire-wall cooling and heating destabilize and stabilize the second mode in hypersonic boundary-layers [4,12,43], and it seems that the thermal strip causes similar influences on far downstream region. The analyses carried out in this study reveal that, regardless of the heating/cooling type, a localized temperature variation can cause both locally greater and smaller N-factor envelopes around the strip. Thus, the results imply that an appropriate arrangement of them can be considered to control the onset of transition.

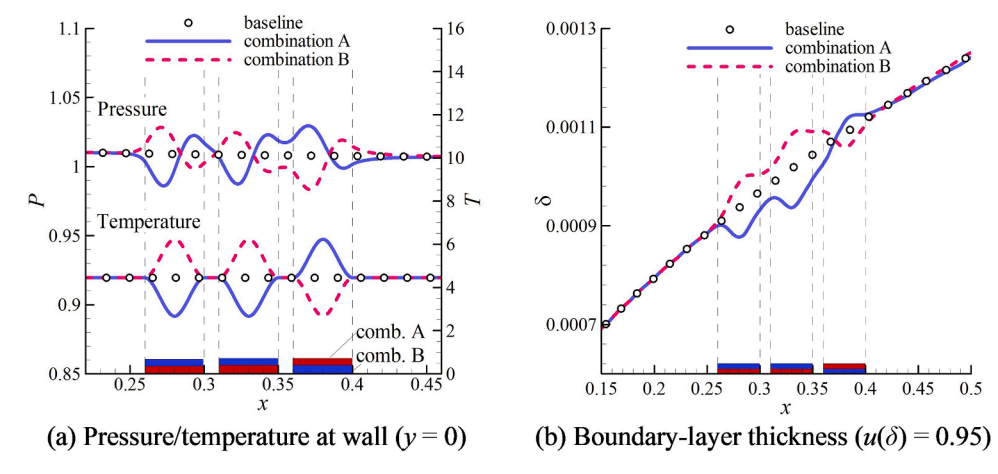
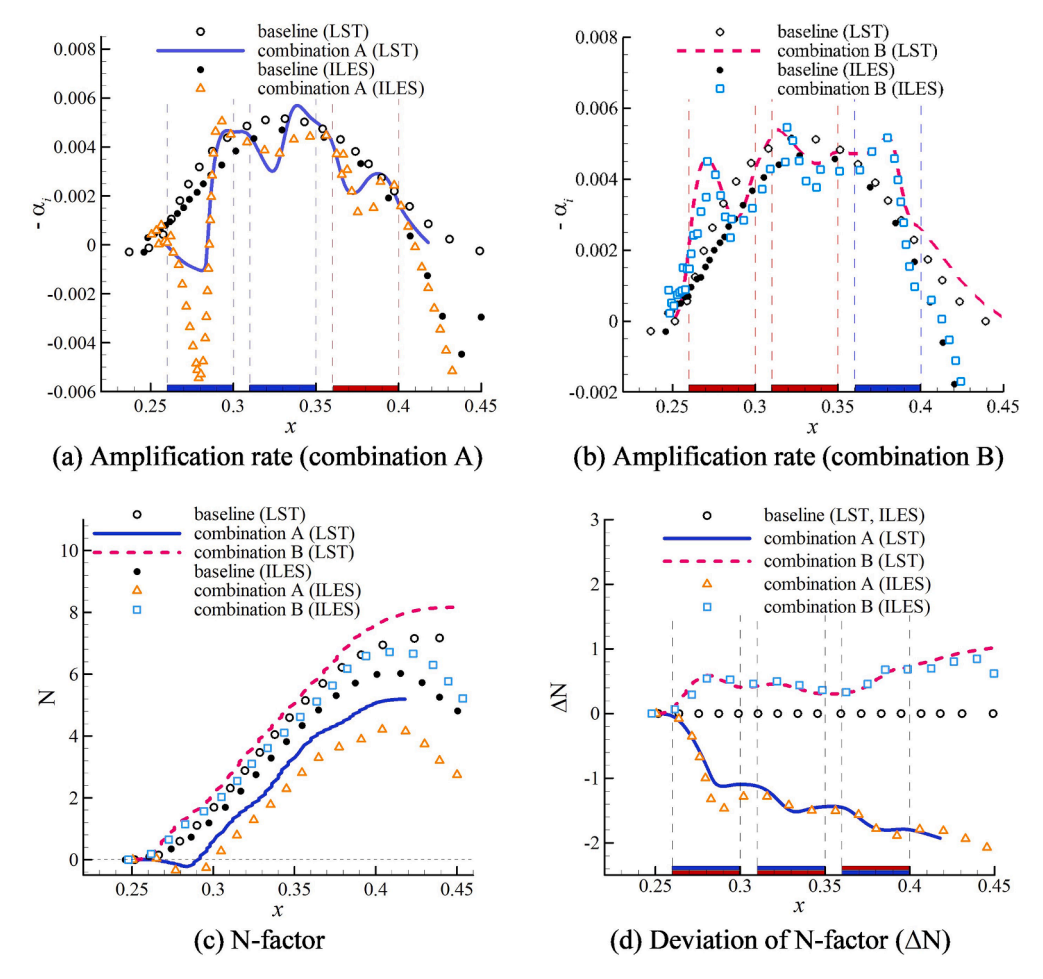
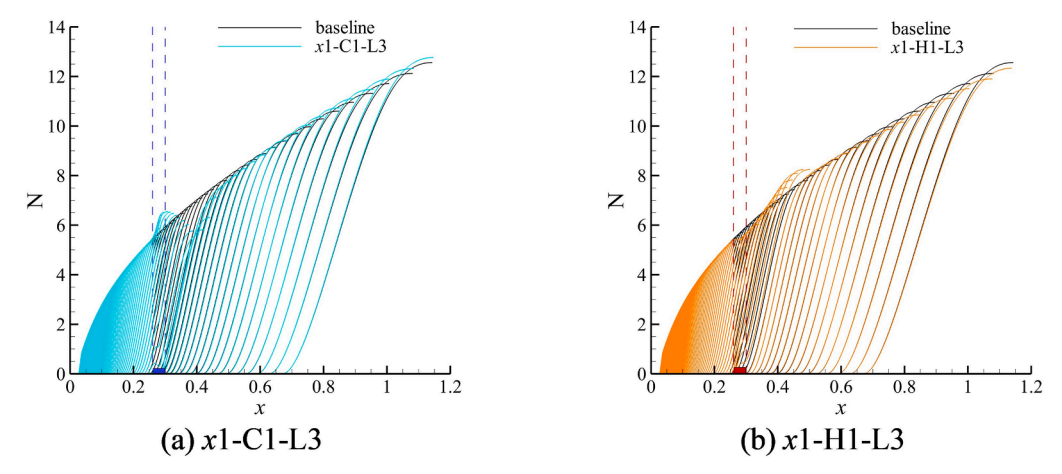


Fig. 18. Comparison of mean flow for strip combinations.



**Fig. 19.** Comparison of stability analysis results for strip combinations (F = 50).

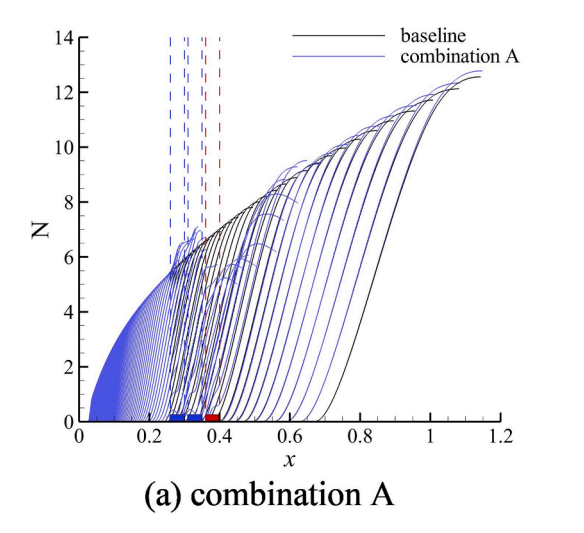


**Fig. 20.** N-factor curves for a single heating/cooling strip (F = 30 - 150).

The overall influence of strip combinations is also examined. The N-factor envelopes are compared in Fig. 21 together with the baseline case. It can be seen from Fig. 21a that combination A, which was intended to stabilize the instability wave of F=50, makes the boundary layer more unstable in the region of the first two cooling strips. The stabilization effect is attainable downstream of the two cooling strips. Subsequently, the envelope experiences an abrupt increase at approximately x=0.5, representing the destabilization with an overshoot at around x=0.6. This variation is attributed to the reversal phenomenon and the different thermal type assigned for the third strip. For combination A, where the

cooling area is larger than the heating region, the envelope exhibits slightly greater(unstable) values compared to the baseline case in the far downstream region. (see Fig. 21a) Similar but opposite features are observed for combination B, as shown in Fig. 21b. The intended stabilizing/destabilizing effects on the N-factor envelope emerge only after the first two cooling/heating strips. The boundary layer is slightly destabilized/stabilized further downstream of the unstable region for combinations A and B, respectively.

Regardless of the number of strips and their type, the hypersonic boundary-layer would experience both stabilizing and destabilizing



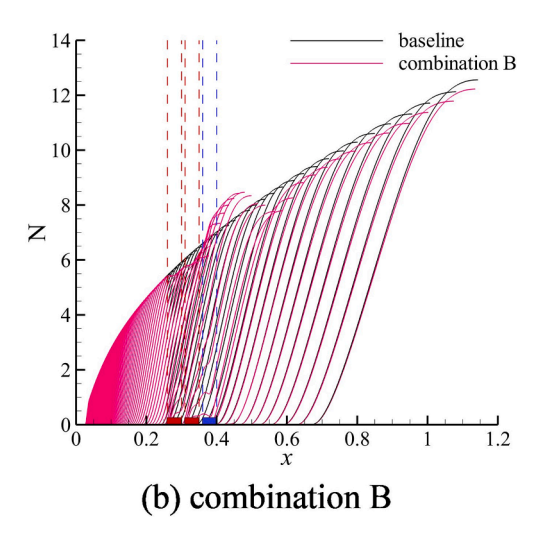


Fig. 21. N-factor curves for combinations of heating/cooling strips.

influences throughout the entire region. Therefore, selecting the locations, thermal types, and intensities of thermal strips is crucial for achieving the desired control effectiveness on the boundary-layer transition for a specific flow condition and configuration.

#### 4. Conclusion

The effectiveness of heating/cooling strips on the evolution of second-mode instability was investigated for the hypersonic boundary-layer over a flat plate at M=4.5. The influences of a single strip and combinations of them were investigated in detail. The LST results were compared with the ILES results for several selected cases to validate the analysis method. Fairly good agreements were confirmed in the general tendency and qualitative behavior of the amplification rates. The reversal of stabilization/destabilization effect according to wall temperature-induced streamwise compression and expansion was identified and discussed in terms of the location of the strip's center relative to the reversal point. The following three conclusions are derived:

(1) The compression and expansion in the streamwise direction are induced, owing to the wall-temperature variation. The flow experiences a series of compression and expansion sequentially around the thermal strip as passing over it. The compression and expansion are formed near the region of a positive and negative temperature gradient, respectively. Thus, the thermal type of strip (heating or cooling) determines the order of the compression or expansion. The compression or expansion formed near the leading edge of the strip is stronger than the one that follows. The change in the boundary-layer thickness around the heating strip possesses very similar characteristics to that formed around a smooth hump reported in previous studies.

(2) The effect of the streamwise pressure gradient induced by a wall-temperature variation on the second-mode instability is reversed when the location of the strip is moved downstream beyond a certain threshold location. The streamwise compression formed upstream from the reversal point makes the instability wave unstable, whereas that formed downstream from this point causes the opposite effect. The reversal point is located downstream of the synchronization point and very close to the location of the maximum growth rate of the second-mode instability. This observation represents a consistent feature with that made in literature [10]. Thus, the reversal phenomenon can result in a different effect on the overall amplification even for the same strip, depending on the relative location between the strip's center and the reversal point.

(3) Analyses for a combination of three strips confirmed that applying a properly designed series of strips could achieve a more

significant stabilizing or destabilizing effect on an instability wave with a specific frequency. The arrangement must be designed by keeping in mind the reversal phenomenon to achieve the desired effect on the second-mode instability. The analyses for various frequencies revealed that the thermal strips have both overall stabilizing and destabilizing effects depending on the relative location of the strip to the reversal point of disturbance with various frequencies, regardless of their type or the number of strips. The results imply that the selection of types and arrangements could play an important role in controlling the hypersonic boundary-layer instability and transition. The thermal strips can be considered as one of the candidates for active control strategies to control the transition onset for a specific design flow condition and configuration.

The present study only sheds light on the physical relations of the thermal strips and the second-mode instability. Thus, for further understanding of underlying physics and applying them to predict and control the transition, more realistic wall-temperature variations which can be encountered on the surface of the hypersonic flight vehicles, other instability modes, including the first mode or crossflow instabilities, and non-linear evolutions need to be studied in the future.

# CRediT authorship contribution statement

Jaeyoung Park: Writing – original draft, Methodology, Formal analysis, Data curation, Investigation, Visualization. Prasanna Thoguluva Rajendran: Formal analysis, Software, Methodology. Minwoo Kim: Methodology, Validation. Jiseop Lim: Methodology. Solkeun Jee: Supervision, Funding acquisition. Donghun Park: Conceptualization, Software, Writing – review & editing, Supervision, Funding acquisition.

# **Declaration of Competing Interest**

The authors declare that there are no competing interests that have influenced this work.

# Data availability

Data will be made available on request.

# Acknowledgement

This work was supported by the National Research Foundation of Korea (NRF) grant funded by the Korean government

(2020R1C1C101318512). This work was also supported by the National Research Foundation of Korea (NRF) grant funded by the Ministry of Science and ICT (MIST) of the Korean government (NRF-2017M1A3A3A02016810).

#### References

- Johnson H, Candler G. Hypersonic boundary layer stability analysis using PSE-Chem. In: 35th AIAA Fluid Dynamics Conference and Exhibit; 2005. https://doi. org/10.2514/6.2005.5023
- [2] Van Driest E. Investigation of laminar boundary layer in compressible fluids using the Crocco method. NACA Tech 1952. https://digital.library.unt.edu/ark: /67531/metadc56237/
- [3] Mack L. Boundary-layer linear stability theory. AGARD Rep. 709. 1984, https://apps.dtic.mil/sti/citations/ADP004046.
- [4] Masad J, Abid R. On transition in supersonic and hypersonic boundary layers. International journal of engineering science 1995;33(13):1893–919. https://doi. org/10.1016/0020-7225(95)00046-Z.
- [5] Soudakov V, Egorov I, Fedorov A. Numerical simulation of receptivity of a hypersonic boundary layer over a surface with temperature jump. In: 6th European Symposium on Aerothermodynamics for Space Vehicles; 2009. https://ui.adsabs. harvard.edu/abs/2009ESASP.659E.66S/abstract.
- [6] Sidorenko A, Gromyko Y, Bountin D, Polivanov P, Maslov A. Effect of the local wall cooling/heating on the hypersonic boundary-layer stability and transition. Progress in Flight Physics 2015;7:549–68. https://doi.org/10.1051/eucass/201507549.
- [7] Fedorov A, Soudakov V, Egorov I, Sidorenko A. High-speed boundary-layer stability on a cone with localized wall heating or cooling. AIAA J 2015;53(9): 2512–24. https://doi.org/10.2514/1.J053666.
- [8] Zhao R, Wen C, Tian X, Long T, Yuan W. Numerical simulation of local wall heating and cooling effect on the stability of a hypersonic boundary layer. International Journal of Heat and Mass Transfer 2018;121:986–98. https://doi.org/10.1016/j. iiheatmasstransfer.2018.01.054.
- [9] Batista A, Kuehl J. Local wall temperature effects on the second-mode instability. Journal of Spacecraft and Rockets 2020;57(3):580–95. https://doi.org/10.2514/1. A34620.
- [10] Zhao L, Dong M. Effect of surface temperature strips on the evolution of supersonic and hypersonic Mack modes: Asymptotic theory and numerical results. Physical Review Fluids 2022;7(5):053901. https://doi.org/10.1103/ PhysRevFluids.7.053901.
- [11] Park D, Park S. Study of effect of a smooth hump on hypersonic boundary layer instability. Theoretical and Computational Fluid Dynamics 2016;30(6):543–63. https://doi.org/10.1007/s00162-016-0396-7.
- [12] Fedorov A, Tumin A. High-speed boundary-layer instability: old terminology and a new framework. AIAA J 2011;49(8):1647–57. https://doi.org/10.2514/1. 1050835
- [13] Kendall J. Wind tunnel experiments relating to supersonic and hypersonic boundary-layer transition. AIAA J 1975;13(3):290–9. https://doi.org/10.2514/ 3.49694.
- [14] Jaffe N, Okamura T, Smith A. Determination of spatial amplification factors and their application to predicting transition. AIAA J 1970;8(2):301–8. https://doi. org/10.2514/3.5660.
- [15] Johnson H, Seipp T, Candler G. Numerical study of hypersonic reacting boundary layer transition on cones. Physics of Fluids 1998;10(10):2676–85. https://doi.org/ 10.1063/1.869781.
- [16] Johnson H, Candler G. Analysis of Laminar-Turbulent Transition in Hypersonic Flight Using PSE-Chem. In: 36th AIAA Fluid Dynamics Conference and Exhibit; 2006. https://doi.org/10.2514/6.2006-3057.
- [17] Fong K, Wang X, Zhong X. Numerical simulation of roughness effect on the stability of a hypersonic boundary layer. Computers & Fluids 2014;96:350–67. https://doi. org/10.1016/j.compfluid.2014.01.009.
- [18] Kim M, Lim J, Kim S, Jee S, Park J, Park D. Large-eddy simulation with parabolized stability equations for turbulent transition using OpenFOAM. Computers & Fluids 2019;189:108–17. https://doi.org/10.1016/j.compfluid.2019.04.010.
- [19] Lim J, Kim M, Park J, Kim T, Jee S, Park D. Simulation of hypersonic boundary layer on porous surfaces using OpenFOAM. Computers & Fluids 2022;240:105437. https://doi.org/10.1016/j.compfluid.2022.105437.
- [20] Lim J, Kim M, Kim S, Jee S, and Park D. PSE-Coupled LES Method for Turbulent Transition in Compressible Boundary Layer. In: AIAA SCITECH 2022 Forum 2022, 10.2514/6.2022-0476.

- [21] Boris J. On large eddy simulation using subgrid turbulence models Comment 1. In: Whither turbulence? Turbulence at the crossroads; 1990. https://doi.org/10.1007/ 3-540-52535-1 53
- [22] Lesieur M, Metais O. New trends in large-eddy simulations of turbulence. Annual review of fluid mechanics 1996;28(1):45–82. https://www.annualreviews.org/ doi/pdf/10.1146/annurev.fl.28.010196.000401.
- [23] Tufis M, Bisek N, Kimmel R. Implicit Large-Eddy Simulation of Discrete Roughness Boundary-Layer Transition with Added Perturbations. In: AIAA Aviation 2019 Forum; 2019. https://doi.org/10.2514/6.2019-2967.
- [24] Li C. A compressible solver for the laminar-turbulent transition in natural convection with high temperature differences using implicit large eddy simulation. International Communications in Heat and Mass Transfer 2020;117:104721. https://doi.org/10.1016/j.icheatmasstransfer.2020.104721.
- [25] Parent B. Positivity-preserving dual time stepping schemes for gas dynamics. Journal of Computational Physics 2018;361:391–411. https://doi.org/10.1016/j.icp.2018.01.046
- [26] Roe P. Approximate Riemann solvers, parameter vectors, and difference schemes. Journal of computational physics 1981;43(2):357–72. https://doi.org/10.1016/0021-9991(81)90128-5.
- [27] Anderson W, Thomas J, Van Leer B. Comparison of finite volume flux vector splittings for the Euler equations. AIAA J 1986;24(9):1453–60. https://doi.org/ 10.2514/3.9465.
- [28] Balsara D, Garain S, Shu C. An efficient class of WENO schemes with adaptive order. Journal of Computational Physics 2016;326:780–804. https://doi.org/ 10.1016/j.jcp.2016.09.009.
- [29] Nayfeh A, Ragab S, Al-Maaitah A. Effect of bulges on the stability of boundary layers. The Physics of fluids 1988;31(4):796–806. https://doi.org/10.1063/ 1.866815
- [30] Masad J, Iyer V. Transition prediction and control in subsonic flow over a hump. Physics of Fluids 1994;6(1):313–27. https://doi.org/10.1063/1.868086.
- [31] Iyer V, Harris J. Computation of three-dimensional compressible boundary layers to fourth-order accuracy on wings and fuselages. In: 27th Aerospace Sciences Meeting; 1989. https://doi.org/10.2514/6.1989-130.
- [32] Ma Y, Zhong X. Receptivity of a supersonic boundary layer over a flat plate. Part 1. Wave structures and interactions. Journal of Fluid Mechanics 2003;488:31–78. https://doi.org/10.1017/S0022112003004786.
- [33] Ma Y, Zhong X. Receptivity of a supersonic boundary layer over a flat plate. Part 2. Receptivity to free-stream sound. Journal of Fluid Mechanics 2003;488:79–121. https://doi.org/10.1017/S0022112003004798.
- [34] Tumin A, Zhong X, Zhong X. Numerical simulation and theoretical analysis of perturbations in hypersonic boundary layers. AIAA J 2011;49(3):463–71. https://doi.org/10.2514/1.J050431.
- [35] Wang X, Zhong X. Effect of wall perturbations on the receptivity of a hypersonic boundary layer. Physics of fluids 2009;21(4):044101. https://doi.org/10.1063/ 1.3103880.
- [36] Wang X, Zhong X, Ma Y. Response of a hypersonic boundary layer to wall blowingsuction. AIAA J 2011;49(7):1336–53. https://doi.org/10.2514/1.J050173.
- [37] Park D, Park S. Influence of two-dimensional smooth humps on linear and non-linear instability of a supersonic boundary layer. Computers & Fluids 2013;79: 140–9. https://doi.org/10.1016/j.compfluid.2013.03.018.
- [38] Park D, Park S. Linear and non-linear stability analysis of incompressible boundary layer over a two-dimensional hump. Computers & Fluids 2013;73:80–96. https://doi.org/10.1016/j.compfluid.2012.12.007.
- [39] Fong K, Wang X, Zhong X. Parametric study on stabilization of hypersonic boundary layer waves using 2-D surface roughness. In: 53rd AIAA Aerospace Sciences Meeting; 2015. https://doi.org/10.2514/6.2015-0837.
- [40] Egorov I, Fedorov A, Soudakov V. Direct numerical simulation of disturbances generated by periodic suction-blowing in a hypersonic boundary layer. Theoretical and Computational Fluid Dynamics 2006;20(1):41–54. https://doi.org/10.1007/ s00162-005-0001-v.
- [41] Wang X, Zhong X. The stabilization of a hypersonic boundary layer using local sections of porous coating. Physics of fluids 2012;24(3):034105. https://doi.org/ 10.1063/1.3694808
- [42] Wang X, Zhong X. Role of the synchronization point on boundary layer stabilization using porous coating. In: 38th Fluid Dynamics Conference and Exhibit; 2008. https://doi.org/10.2514/6.2008-4382.
- [43] Chang C, Kline H, Li F. Wall Cooling Effect on High-Enthalpy Supersonic Modes over a Cone. AIAA J 2021;59(10):3831–44. https://doi.org/10.2514/1.J060161.